RESEARCH PAPER

Evaluation of Cation-Mediated Wound Healing Effects in Honey-Based Gel Formulations

Mohammed Mukhtar Alghadeer[1], Pooja Gudennavar[2], Nagesh Chandrasekhara Setty[2*], Sunil Attimarad[2], Sibghatullah Muhammad Ali Sangi[3], Krishna Swaroop[4*], Sreeharsha Nagaraja[1], Giresh Meravanige[4], Pavan Kumar Pavagada Sreenivasalu[5*]

[1]Department of Pharmaceutical Sciences, College of Clinical Pharmacy, King Faisal University, Al Ahsa, Saudi Arabia

[2]Department of Pharmaceutics, Maratha Mandal's College of Pharmacy, Belagavi-590016, Karnataka, India

[3]Basic Medical Sciences Department, College of Medicine, Dar Al Uloom University, Riyadh, Saudi Arabia

[4]Department of Biomedical Sciences, College of Medicine, King Faisal University, Al-Ahsa 31982, Saudi Arabia

[5]Department of Restorative Dental Sciences, College of Dentistry, King Faisal University, Al Ahsa, Saudi Arabia

Corresponding Authors:

Dr. Nagesh C

Professor and HOD, Department of Pharmaceutics, Maratha Mandal's College of Pharmacy, Belagavi-590016, Karnataka, India

Email: nagesh1273@gmail.com

Dr. Krishna Swaroop

Department of Biomedical Sciences, College of Medicine, King Faisal University, Al-Ahsa 31982, Saudi Arabia

Email: ksreehari@kfu.edu.sa

Dr. Pavan Kumar Pavagada Sreenivasalu

Department of Restorative Dental Sciences, College of Dentistry, King Faisal University, Al Ahsa, Saudi Arabia

ABSTRACT

The aim of the study was to evaluate the efficacy of honey gel-based wound care preparation using nanoparticles (NPs) of zinc oxide (ZnO) and iron oxide (Fe_2O_3) to facilitate wound healing. ZnO-NPs and Fe_2O_3-NPs were synthesized by the precipitation method and their concentration, pH, and temperature were optimized. Particle size, zeta potential, FTIR, SEM, and UV-visible spectroscopy were used in the characterization process. Escherichia coli (E. coli) and Staphylococcus aureus (S. aureus) were tested for antibacterial activity using the MIC technique. Optimized NPs were incorporated with carbopol 934 in a honey-based gel and evaluated for various physicochemical parameters. A wound healing efficacy model was conducted in Wistar albino rats using an excision wound model and the results were supported by histological tests. The ZnO-NPs had an absorbance peak at 357 nm, a mean particle size of 157.1 nm, and a zeta potential of 14.4 mV, indicating they are very stable. The Fe_2O_3-NPs absorbed the light at 300 nm, with a size of 186.8 nm and a zeta potential of 12.6 mV. SEM analysis showed ZnO-NPs to be spherical and Fe_2O_3-NPs irregular in shape, with both exhibiting significant antimicrobial activities. The activity of these NPs was found to be broad-spectrum, as indicated by MIC values. In vivo studies revealed that honey gels loaded with NPs significantly enhanced wound contraction compared to the control and plain gel groups ($p < 0.05$). By day 21, the ZnO-NPs gel and Fe_2O_3-NPs gel achieved wound contraction rates of $99.44 \pm 0.06\%$ and $99 \pm 0.11\%$, respectively. Histopathological analysis showed complete re-epithelialization, increased collagen deposition, and reduced inflammatory infiltration in the treated groups. The study shows that honey-based gels containing ZnO-NPs and Fe_2O_3-NPs significantly enhanced healing of wounds and antibacterial effects in comparison with the control group. The combination of metal oxide nanoparticles and honey makes these compositions potential candidates for topical wound treatment.

Keywords: Zinc oxide nanoparticles; Iron oxide nanoparticles; Honey-based gel; Wound healing; Excision wound model; Histopathology.

How to cite this article: Alghadeer MM, Gudennavar P, Setty NC, Attimarad S, Sangi SMA, Swaroop K, Nagaraja S, Meravanige G, Sreenivasalu PKP. Evaluation of Cation-Mediated Wound Healing Effects in Honey-Based Gel Formulations. Int J Drug Deliv Technol. 2026;16(9s): 57-67; DOI: 10.25258/ijddt.16.9s.7

INTRODUCTION

A wound is defined as a lesion caused by accidental trauma or sharp objects that disrupts tissue's cellular and anatomical continuity, regardless of infection status. These injuries might be created by chemical, physical, mechanical, microbiological, or immune-related injury.[1] Wounds are a major clinical issue, affecting around 2.5 % of the US population and inflicting a huge economic burden on healthcare systems, with projected yearly Medicare expenses ranging from 28.1 to 96.8 billion USD.[2] Chronic and non-healing wounds are becoming more common as people become older, develop diabetes, and gain weight, all of which slow down normal wound repair mechanisms.[3] Wound healing is a multifaceted, well-coordinated physiological process that includes a wide range of cellular, pathophysiological, and immunological mediators.[4] It involves four interconnected phases, namely haemostasis, inflammation, proliferation, and remodelling. To control bleeding, haemostasis requires platelet aggregation and the production of fibrin clots. Inflammation follows, during which both macrophages and neutrophils remove debris and pathogens while generating cytokines that start the healing process.[5] The proliferation phase is distinguished by fibro-blast activity, collagen deposition, angiogenesis, and re-epithelialization.[6] Finally, during remodelling, collagen III is replaced with collagen I, resulting in greater tensile strength and scar maturatio.[7] Various therapeutic techniques are used to promote wound healing, ranging from traditional wound cleansing, debridement, and dressings to advanced pharmacological and regenerative therapies.[8,9,10] Natural products, such as aloe vera and plant extracts, are also in demand due to their antibacterial as well as therapeutic propertie.[11] Nevertheless, the conventional dressings do not offer much protection, and prolonged use of antibiotics may result in resistance and systemic side effect.[12]

Metal ions, e.g. zinc and iron, help in wound healing by promoting cell growth, collagen, angiogenesis, and antimicrobial protection.[3] Zinc is involved in the migration of keratinocytes, cell growth, and re-epithelialization and has been extensively known to have antibacterial and anti-inflammatory effects.[13,14] Iron helps in transporting oxygen to the body, cellular metabolism, collagen formation, and angiogenesis, which facilitate tissue regeneration during the inflammatory and proliferation phases.[15,16,17] However, because these ions are unstable and quickly eliminated in their free forms, their therapeutic efficacy is limited. The delivery systems developed by NPs overcome these limitations and enhance the stability of therapeutic ions and bioavailability, as well as the sustained release. The NPs enhance the healing in wounds by enhancing tissue penetration and cellular contact and limiting the systemic toxicity because they are small and have a high surface-area-to-volume ratio.[18] The zinc and iron were chosen for their established wound-healing capability and are produced in the form of oxide NPs in this study. Zinc and iron have benefits over other metal oxides, including better safety profiles, lesser risk of cytotoxicity, lower cost, high chemical stability, and significant physiologic functions in tissue repair. Silver NPs are excellent antimicrobials, but prolonged exposure causes cytotoxicity and delayed epithelialization, whereas copper NPs can cause oxidative stress at high doses.[13,14,19]

Honey is among the popular natural wound healers since it possesses broad-spectrum antibacterial, anti-inflammatory, and antioxidant effects. Honey-based gels are a combination of these therapeutic advantages and a semi-solid dosage form that enables the gels to stay in contact with the wound surface longer, controlled release of bioactive chemicals, and higher compliance by the patient. These compounds augment fibroblast growth and deposition of collagen, decrease microbial load, and are applicable in the current wound care.[20,21,22] Also, honey has antimicrobial properties, low pH, osmotic effect, and hydrogen peroxide production, which can be used synergistically with metal oxide NPs to produce synergistic effects that can maximize the effect of NPs-mediated mechanisms such as membrane disruption, reactive oxygen species (ROS) generation, and sustained ion release. In addition to speeding up tissue regeneration and lowering inflammation, this synergy can improve antibacterial activity. [23,24] Therefore, in the present work, Zn and Fe ions are converted into ZnO-NPs and Fe_2O_3-NPs, and characterized for various parameters. Then the optimized NPs were incorporated into honey-based gel, and their potential to accelerate wound healing was assessed.

MATERIALS AND METHODS

Materials

Analytical-grade chemicals were utilized. Zinc acetate dihydrate ($Zn(CH_3CO_2)_2 \cdot 2H_2O$) and sodium hydroxide (NaOH) of analytical grade were purchased from Molychem Pvt. Ltd., and SD Fine-Chem Ltd., Mumbai, India. ferrous sulphate ($FeSO_4$) was bought from Nice Chemicals Pvt. Ltd., India. ethanol was sourced from Loba Chem Pvt. Ltd., Mumbai. carbopol

934, methyl paraben, and propyl paraben were provided by Hi Media Laboratories Pvt. Ltd., Mumbai. triethanolamine (TEA) was purchased from SD Fine-Chem Ltd., in Mumbai. The gel base was prepared using natural honey from a reliable local provider.

Method of preparation of ZnO-NPs and Fe_2O_3-NPs

Zinc acetate dihydrate and sodium hydroxide were used as precursors for the synthesis of ZnO-NPs via the direct precipitation method. Ethanol was used as the solvent for the preparation. In this experiment, a 7.22 mMol ethanol solution of sodium hydroxide was added dropwise to a 3.73 mMol aqueous ethanol solution of zinc acetate dihydrate under high-speed stirring for 2.25 hours under standard conditions at a 60 °C synthesis temperature, resulting in white turbidity; after that, it was allowed to reach room temperature. After removing the supernatant solution, the precipitated zinc oxide was centrifuged for 20 minutes at 5000 rpm and then repeatedly cleaned with pure ethanol to get rid of any undesirable compounds that were attached to NPs. The ZnO-NPs were then dried at 60 °C for 2 hours or redispersed in ethanol, and they were stored at room temperature. The reaction was carried out under alkaline conditions (pH 10) with continuous stirring to ensure controlled nucleation and growth of NPs.

A similar procedure was utilized to synthesize Fe_2O_3-NPs, with the exception that $FeSO_4$ was used as the precursor rather than zinc acetate dihydrate, and the reaction was performed under the same alkaline conditions (pH 10) with continuous stirring at 60 °C for uniform NPs formation. The formation of Fe_2O_3-NPs was indicated by the appearance of a dark greenish precipitate.[25,26]

Characterization of ZnO-NPs and Fe_2O_3-NPs

Ultraviolet-visible spectral analysis

The formation of NPs was confirmed using a UV-visible spectrophotometer (LABINDIA ANALYTICAL UV 3200) in the 200-800 nm wavelength range. Before analysis, the dry powders of ZnO-NPs and Fe_2O_3-NPs were dispersed in Milli-Q water and sonicated using a bath sonicator for 10 minutes prior to UV-vis measurement.[27]

Fourier transform infrared spectroscopy (FT-IR)

The compatibility of the excipients in the formulation was determined using FT-IR. A spectrometer (Perkin Elmer Spectrum 100-FTIR, USA) was used to analyse the FT-IR spectra of ZnO-NPs, Fe_2O_3-NPs, and NaOH between the 400-4000 cm^{-1} range, using the KBr pellet method for sample preparation.[28]

Particle size and zeta potential analysis

The particle size distribution, particle size, and zeta potential of the produced ZnO-NPs and Fe_2O_3-NPs were evaluated using the DLS technique on a Zetasizer instrument (Horiba SZ-100). The dry powders of ZnO-NPs and Fe_2O_3-NPs were uniformly dispersed in Milli-Q water with an ultrasonic bath at 40 kHz for 1 minute at room temperature.[29]

Scanning electron microscopy (SEM)

The morphology/shape of ZnO-NPs and Fe_2O_3-NPs was investigated using a scanning electron microscope (JSM-IT810, JEOL Ltd., Japan) operated at an accelerating voltage of 15 kV, with a resolution of 60 Å and appropriate magnifications.[24]

Minimum Inhibitory Concentration (MIC)

The antibacterial activity of the synthesized test sample was determined using the resazurin assay technique. Resazurin (270 mg) was dissolved in 40 mL of sterile distilled water for the experiment. To ensure that the solution was uniform and completely dissolved, a vortex mixer was used. The experiments were conducted aseptically in a 96-well plate. To start, pipette 100 µL of dimethyl sulphoxide (7.8, 15.6, 31.2, 62.5, 125, 250, 500, 1000 µg/mL) into the plate well. After that, add 50 µL of nutritional broth to each well and dilute it. Resazurin indicator solution (10 µL) was added to each well. Each well received 10 µL of a fungal or bacterial solution. Streptomycin (7.8, 15.6, 31.2, 62.5, 125, 250, 500, and 1000 µg/mL) was used as a standard control. Cling film was applied lightly in each of the dishes to prevent the drying of the bacteria. The plate was then incubated for 18-24 hours at 37 °C, and the color change was seen visually. Any color changes from blue to pink or colorless were classified as positive, while the absence of color shift was classified as negative. The absorbance of the plate was measured at 600 nm with an ELISA reader. The percentage of inhibition was estimated using the following formula.[30]

$$\% \text{ of Inhibition} = \left(\frac{\text{Test}}{\text{Control}}\right) * 100$$

Preparation of Honey-Based Gel containing ZnO-NPs and Fe_2O_3-NPs

Carbopol was dispersed in purified water with steady stirring to make honey-based hydrogel, which was then neutralized with triethanolamine, and preservatives

such as methyl paraben and propyl paraben were added. After allowing the mixture to swell for a full day at room temperature, then honey was added with continuous stirring. In order to establish a uniform formulation, ZnO-NPs and Fe_2O_3-NPs were added to the gel base after being dispersed in a small amount of water (Table 1).[31]

Table No. 1: Formulation of honey-based nanoparticle gel

Sr. no.	Ingredients	Quantity for Honey-Based Gel containing ZnO-NPs	Quantity for Honey-Based Gel containing Fe_2O_3-NPs
1	NPs	1 gr	1 gr
2	Carbopol 940	1% w/w	1% w/w
3	Honey	37.5 gr	37.5 gr
4	Triethanolamine (TEA)	0.3% w/w	0.5% w/w
5	Methyl paraben	0.18 %	0.18 %
6	Propyl paraben	0.02 %	0.02 %
7	Distilled water	Quantity Sufficient	Quantity Sufficient

Evaluation of honey-based gel

Visual examination

Visually inspect honey compositions for color, consistency, homogeneity, and lumps after storage.[23]

Determination of pH

A calibrated digital pH meter was used to determine the pH of the gel formulation. One gram of gel was mixed into 100 milliliters of freshly prepared distilled water, and the electrode was immersed in the solution for 10 minutes before the pH was measured. The equipment was calibrated before testing with standard buffer solutions at pH 4.0, 7.0, and 10.0.[32]

Determination of Viscosity

A Brookfield digital viscometer was used to measure the viscosity of the gel. Spindle number 64 at 10 rpm and 25 °C was used to measure the viscosity. Before measurement, the gel was deaerated and placed in a suitable wide-mouth container. Gel samples were settled for 30 minutes at assay temperature (25 ± 10 °C) before measurements.[33]

Spreadability

The honey-based gel's spreadability was evaluated on laboratory-built glass slides. The lower glass slide had 1 gram of gel on it, while the second slide had a standard weight on top. Spreadability was determined by timing how long it took for the upper and lower slides to separate.[34]

***In vivo* Wound healing study**

Wound healing activity using an animal model

The Maratha Mandal College of Pharmacy's Institutional Animal Ethics Committee granted prior approval for the animal studies (Approval No.: MMCP/2024-25/B.Ph/11). The wound-healing activities were carried out using 24 Wistar albino rat models. The following five groups ($n = 3$) were created from adult rats weighing 150-200 g: Group 1 was a control group that was injured and given saline solution treatment; Group 2 was a marketed product that was treated with silver sulfadiazine; Group 3 was plain gel; Group 4 was a formulated honey-based gel that contained ZnO-NPs; and Group 5 was a formulated honey-based gel that contained Fe_2O_3-NPs. Each rat's dorsal region was shaved with an electric trimmer the day before the experiment. Using forceps and surgical scissors, an excision was made on the dorsal spinal area after anaesthesia was established using the open-mask technique with anaesthetic ether. An appropriate amount of gel was applied daily on the wound throughout the study period. Following the application, each rat was kept in a cage at room temperature. Four weeks later, the damaged skin tissue was removed, stored in 10 % formalin, and examined histopathologically.[35]

Determination of wound contraction

On days 0, 4, 8, 12, 16, and 21, the excision wounds were traced onto millimetre-scale graph paper to determine the wound area. The wound area was measured every fourth day to determine wound contraction, which was expressed as a percentage reduction until complete healing occurred.[36]

$$\text{Wound closure percentage} = \frac{\text{Initial wound size} - \text{Specific day wound size}}{\text{Initial wound size}} \times 100$$

Determination of epithelialization period

The removal of dead issue without any additional raw wound was deemed the endpoint of complete epithelization, and the day required for this was designated the epithelialization period.[37]

Histopathology study

Each group of rats had a sample of wound tissue taken from their skin, which was stored in 10 % buffered

formalin. Following standard processing, 5 µm-thick tissue slices were created and stained with haematoxylin and eosin. The stained sections were rated according to the degree of epidermal migration after being qualitatively inspected under a light microscope.[38,39]

Statistical analysis

The average values along with their standard error are presented in this paper. The experiments were conducted in triplicate (n=3). A significant result was defined as $p < 0.05$.[40]

Stability studies

The honey-based gel's stability test was carried out in compliance with ICH regulations. For a maximum of three months, the formulations were observed at 40±2°/75±5%. The gel's appearance, pH, and viscosity have been determined after 1, 2, and 3 months.[41]

RESULTS AND DISCUSSION

Visual Observation

The formation of ZnO-NPs was clearly noticed through a change in the color of the solution, resulting in the formation of a white precipitate upon further stirring. The formation of Fe_2O_3-NPs was visible as a change in the color of the solution from pale yellow to a dark greenish precipitate.

UV-Visible Spectral Analysis

Fig. 1 (A, B) illustrates UV-visible absorption spectra for ZnO-NPs and Fe_2O_3-NPs synthesized by the chemical reduction method. A sharp absorption peak at 357 nm confirmed the successful formation of ZnO-NPs. The absorption peak of Fe_2O_3-NPs at 300 nm confirms their successful formation of Fe_2O_3-NPs. The UV-visible spectroscopic analysis confirmed the synthesis of ZnO-NPs and Fe_2O_3-NPs.

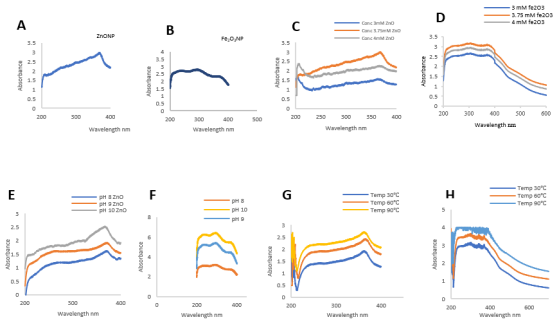

Fig. 1: UV peak of (A) ZnO-NPs (B) Fe_2O_3-NPs; Effect of Concentration (C) ZnO-NPs (D) Fe_2O_3-NPs; Effect of pH (E) ZnO-NPs (F) Fe_2O_3-NPs; Effect of Temperature (G) ZnO-NPs (H) Fe_2O_3-NPs.

Optimization of NPs

In the current investigation, several parameters were tuned, including the concentration of salt, pH of the reaction mixture, and temperature, because these parameters have desirable control over morphological aspects such as particle size and shape, as well as influence NPs production yield. As a result, these properties must be optimized during the NPs manufacturing process.

Effect of Concentration

The concentration of $Zn(CH_3CO_2)_2 \cdot 2H_2O$ plays an important role in determining nanoparticle production and optical characteristics. ZnO-NPs were prepared at various precursor concentrations of $Zn(CH_3CO_2)_2 \cdot 2H_2O$ (3, 3.75, and 4 mM) while maintaining a constant temperature and pH, as shown in Fig. 1(C). Absorption peaks were detected at 352 nm for 3 mM, 357 nm for 3.75 mM, and 355 nm for 4 mM.

Similarly, Fe_2O_3-NPs were prepared at precursor concentrations of $FeSO_4$ (3, 3.75, and 4 mM). Fig. 1(D) shows absorption bands at 298 nm for 3 mM, 300 nm for 3.75 mM (maximum absorbance), and 302 nm for 4 mM. There was no notable shift in peak, showing that aggregation had no major impact on optical properties.

Effect of pH

pH of reaction media is an important element in determining NPs formation and optical characteristics. Similar reaction conditions were investigated by measuring the influence of pH on ZnO-NP generation at pH 8, 9, and 10. The absorption peaks are at 354 nm with pH 8, 356 nm with pH 9, and 357 nm with pH 10 (Fig. 1(E)). The highest intensity of absorbance was reached at pH 10, indicating that alkaline conditions favor ZnO-NPs formation.

On the same note, Fe_2O_3-NPs were produced at pH 8, 9, and 10, and Fig. 1(F) shows comparable UV-vis spectra. For pH 8, 9, and 10, the absorption bands were found at around 298 nm, 300 nm, and 302 nm, respectively. No significant change in peak position was observed, and the maximum absorbance was reached at pH 9, indicating that pH primarily affects NPs stability and growth rather than aggregation.

Effect of Temperature

Another important factor that affects the formation of NPs is temperature. Three distinct temperatures were used to produce ZnO-NPs: 30, 60, and 90 °C. An increase in temperature led to a higher absorbance intensity, as seen in Fig. 1(G), suggesting improved

NPs production at higher temperatures.
Similarly, Fig. 1 (H) shows UV-vis absorption spectra for Fe_2O_3-NPs synthesized at 30, 60, and 90 °C. Temperature had a favorable effect on Fe_2O_3-NPs production, as the absorbance intensity rise with increasing temperature, reaching its peak at 90 °C.

Fourier Transform Infrared Spectroscopy

Fig. 2 (A) shows the FT-IR spectra of ZnO-NPs. The absorption peak at 3300-3500 cm^{-1} is due to the existence of free -OH groups from surface-adsorbed moisture and the reduction process. The peak near 1630 cm^{-1} indicates H-O-H bending vibrations. The significant absorption band below 600 cm^{-1} is related to Zn-O stretching vibrations, confirming the formation of ZnO-NPs. Fig. 2 (B) shows the FT-IR spectra of Fe_2O_3-NPs. Adsorbed water molecules give a large peak at 3400 cm^{-1}, indicating O-H stretching vibrations. The band near 1620-1640 cm^{-1} represents H-O-H bending vibrations. The absorption bands below 600 cm^{-1} are due to Fe-O stretching vibrations, demonstrating the successful formation of Fe_2O_3-NPs. Effective elimination of precursor residues is indicated by the lack of additional peaks that correspond to acetate or sulfate groups, which also validates the purity of the produced NPs.

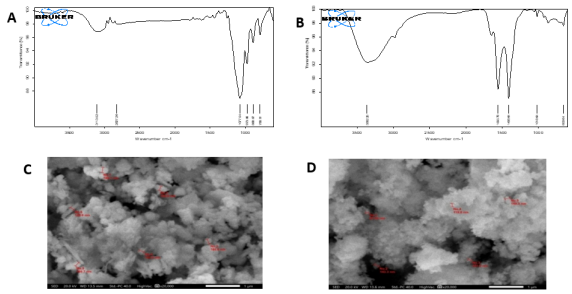

Fig. 2: FT-IR spectra of (A) ZnO-NPs and (B) Fe_2O_3-NPs; SEM images of (C) ZnO-NPs
(D) Fe_2O_3-NPs (Note: the red number denotes the particle size measurement of NPs)

Scanning Electron Microscopy (SEM)

Scanning electron microscopy is demonstrated as a new tool for examining the morphological properties of nanostructures. Fig. 2 (C, D) shows SEM images of ZnO-NPs and Fe_2O_3-NPs, where ZnO-NPs appear uneven and spherical, while Fe_2O_3-NPs show irregular spherical particles with noticeable aggregation. The moderate aggregation seen in SEM images may be due to the comparatively low zeta potential values; yet, the acquired zeta potential indicates appropriate colloidal stability for biological applications.

Particle size and zeta potential analysis

The average particle size, size distribution, and Polydispersity Index (PDI) values for ZnO-NPs and Fe_2O_3-NPs have been determined using the Dynamic Light Scattering technique, as shown in Fig. 3. The Z-average diameter of synthesized ZnO-NPs and Fe_2O_3-NPs was 157.1 nm and 186.8 nm, with PDI values of 0.305 and 0.396, respectively. The zeta potentials of ZnO-NPs and Fe_2O_3-NPs were found to be 14.4 mV and 12.6 mV, respectively.

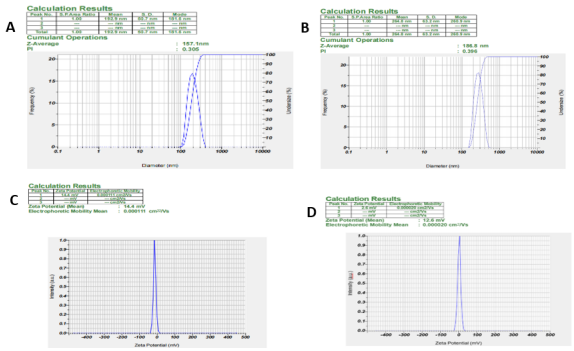

Fig. 3: Particle size distribution of (A) ZnO-NPs and (B) Fe_2O_3-NPs;
Zeta potential of (C) ZnO-NPs (D) Fe_2O_3-NPs

Minimum Inhibitory Concentration (MIC)

ZnO-NPs and Fe_2O_3-NPs were tested for their MIC towards *S. aureus* and *E. coli* bacterial strains. The MIC values show the lowest concentration at which no apparent growth of the test organism was detected. ZnO-NPs had MIC values of 31.2 µg/mL against *S. aureus* and 62.5 µg/mL against *E. coli*. Fe_2O_3-NPs demonstrated MIC values of 62.5 µg/mL against *S. aureus* and 31.2 µg/mL against *E. coli*, as reported in (Table 2).

Table No. 2: Antimicrobial property of sample in MIC

Sr. No.	Microorganism Types	MIC (ZnO-NPs) (µg/mL)	MIC (Fe_2O_3-NPs) (µg/mL)
1	*Staphylococcus aureus*	31.2 µg/mL	62.5 µg/mL
2	*Escherichia coli*	62.5 µg/mL	31.2 µg/mL

According to earlier research on metal oxide NPs, the measured MIC values are comparable, indicating potent antibacterial activity. In order to kill bacteria, the antibacterial mechanism may include the production of reactive oxygen species, membrane rupture, and metal ion release.[42,43]

EVALUATION OF GEL

The optimized NPs were put into a hydrogel mixed with honey, and the following properties were assessed.

Physical examination

Due to the addition of honey in the preparation, the ZnO-NPs gel turned yellow. The recipe produced a smooth, golden gel that was viscous and homogeneous in appearance. Similarly, the Fe_2O_3-NPs gel had a light brown color from the combined effect of honey and NPs, and the texture was creamy, uniform, and consistent.

Measurement of pH

A digital pH meter was used to test the pH of the prepared gel. The ZnO-NP gel had a pH of 5.2 ± 0.15, while the Fe_2O_3-NP gel had a pH of 5.7 ± 0.2. These values are close to the human skin's normal pH, indicating that the compositions are suitable for topical usage without causing irritation. The pH values of all gels are shown in (Table 3).

Viscosity determination

The consistency of the prepared gel is typically correlated with its viscosity. The outcomes can be seen in (Table 3).

Spreadability

Spreading value is another factor that determines a formulation's therapeutic potency. The results for spreadability are shown in (Table 3). The less time it takes to separate gels from slides, the better the spreadability. As a result, all formulations have superior spreadability. The spreadability was observed to increase as the viscosity dropped.

Table No. 3: Study of color, pH, viscosity, and spreadability.

Formulation code	ZnO-NPs gel
Color	yellow
pH	5.2 ± 0.15
Viscosity (cps)	4798 ± 25.8
Spreadability (g.cm/s)	43.6 ± 0.28

Note: Values are expressed as mean ± SD (n=3).

Grittiness

The prepared gel has no lumps or particles, indicating good grittiness.

Homogeneity

The resulting gel is uniform, transparent, and free of any particle matter, clumps, or aggregates.

Animal Activity

Wound healing activity on Wistar rats

The wound healing capacity of honey-based gels made with ZnO-NPs and Fe_2O_3-NPs was tested in a Wistar rat excision wound model. Under anaesthesia, circular excision wounds of 3 mm² were created on the dorsal area of the rats. The animals were treated topically with the individual formulations for 21 days, with wound contraction measured at regular intervals. The wound area was drawn and photographed to assess gradual healing, as illustrated in (Fig. 4). The percentage of wound closure was computed and shown in (Table 4). The results showed that wound contraction increased steadily in the test groups compared to the control. On the 21st day, the control group (saline-treated) showed only 91.66 ± 0.88 % healing, but the standard group (silver sulfadiazine-treated) demonstrated 99.44 ± 0.064 % healing. The plain gel group demonstrated modest healing (84 ±0.40 %), while the test group treated with honey-based gel containing ZnO-NPs and Fe_2O_3-NPs obtained 99.44 ± 0.064 % and 99 ± 0.11 % healing, respectively. When compared to FeO_3-NPs, ZnO-NPs showed marginally better in vivo wound healing performance. This could be because of increased collagen synthesis, zinc-mediated epithelialization, and anti-inflammatory activity, all of which promote tissue regeneration.

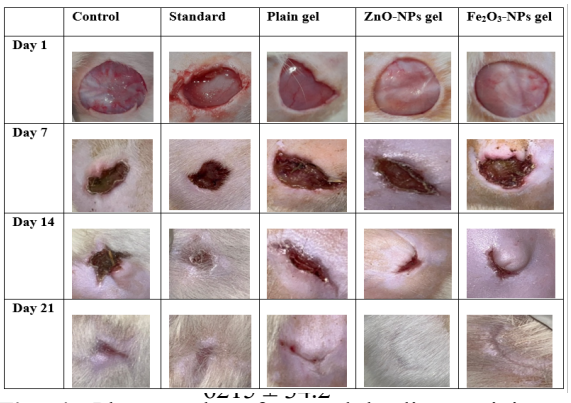

Fig. 4: Photographs of wound healing activity on animal model.

Table No. 4: Effect of formulation on percentage wound contraction in excision wound model.

Groups	Group name	7th Day (%)	14th Day (%)	21st Day (%)

Group 1	Control	17.33±1.34	61.55±0.98	91.66±0.88
Group 2	Standard (silver sulphadiazine)	23.33±1.57	81±0.50	99.44±0.06
Group 3	Plain gel	11.44±0.35	75.44±0.16	84±0.40
Group 4	ZnO-NPs gel	45.55±1.09	88.88±0.8	99.44±0.06
Group 5	Fe_2O_3-NPs gel	38.77±0.89	85±0.33	99±0.11

Note: The values presented are arithmetic mean ± SD of three determinations.

Epithelization period

The epithelization time refers to the moment when a scar has entirely grown. The epithelialization time for group I rats was 18 days, 12 days for group II, 13 days for group III, 11 days for group IV, and 10 days for group V.

Histopathology

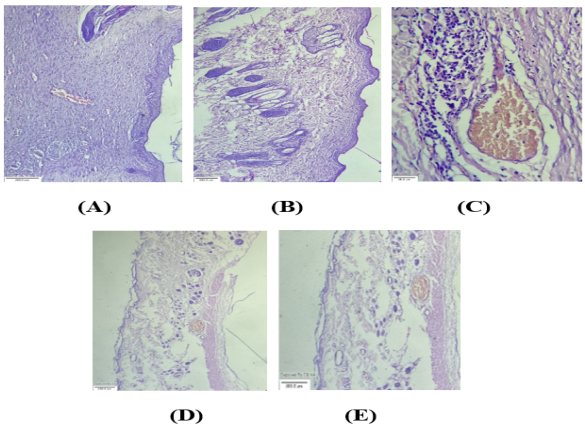

Fig. 5: Histopathology images of (A) Control, (B) Standard, (C) Blank honey-based gel, (D) ZnO-NPs gel, and (E) Fe_2O_3-NPs gel.

The control group had only limited re-epithelialization, modest inflammation, some macrophages, a few fibroblasts, and very little collagen production, indicating sluggish and early-stage healing (Fig. 5A). The standard group showed practically full re-epithelialization, albeit with minor edema and congestion. There was visible fibroblast and fibrocyte activity, enhanced collagen deposition, and adnexal regeneration, indicating more structured and successful repair than the control (Fig. 5B). The Carbopol-honey gel-treated group showed healed epidermis with persisting moderate irritation. Adnexal structures were visible, fibroblast and fibrocyte proliferation was observed, and collagen deposition was minimal, suggesting that wound healing started, but was slower than in the groups treated with NPs (Fig. 5C). Complete re-epithelialization, little inflammation, active fibroblasts and fibrocytes, sufficient collagen deposition, and well-regenerating adnexal structures were all present in the ZnO-NPs gel-treated group, suggesting very successful wound healing and tissue organization (Fig. 5D). Similarly, complete re-epithelialization was attained by the Fe_2O_3-NPs gel-treated group; however, there was quite a bit of discomfort and congestion. Excellent healing was indicated by the abundance of fibroblasts, fibrocytes, and collagen, as well as adnexal regeneration, despite a slight rise in inflammatory response (Fig. 5E). These histological changes are all associated with enhanced collagen deposition, proliferation of fibroblasts, and reduced inflammatory response. This results, in an improved extracellular matrix remodelling and faster tissue regeneration.

Role of honey in wound healing

Honey was found to play an important role in the NPs-based gel formulations to serve as a natural gelling agent and wound healing enhancer. The gels were suitable in terms of being used topically because they were smooth and skin-friendly. Gels containing honey and ZnO-NPs and Fe_2O_3-NPs had an advantage over control groups in healing wounds, contracting and epithelization time, and tissue regeneration. These were observed in a synergistic wound healing response as shown by well-organized epithelium, more collagen deposition, and less inflammation through histopathological analysis.

Stability studies

Stability testing was carried out in accordance with ICH criteria to assure product quality in a variety of environmental circumstances, such as temperature and humidity. ZnO-NPs and Fe_2O_3-NPs gels were kept in plastic airtight containers in a stability chamber at 40 ℃ ± 2 ℃ and 75% ± 5 RH for 3 months. Samples were taken on a regular basis to monitor changes in viscosity, pH, and physical characteristics. The data obtained for ZnO-NPs gel is shown in (Table 5), whereas the data collected for Fe_2O_3-NPs is shown in (Table 6), indicating that there were no notable changes in physical appearance. During the trial period, there was no discernible change in viscosity or spreadability, suggesting that the formulations had good physical stability. As a result, there was no evidence of degradation in the prepared gel.

Table No. 5: Stability study of ZnO-NPs gel

Parameter	ZnO-NPs gel (40 ℃ ± 2 ℃/ 75% ± 5 RH)		
	30 Days	60 Days	90 Days
Color	yellow	yellow	yellow
Odor	No	No	No
pH	5.03 ± 0.2	5.3 ± 0.4	5.11 ± 0.47

Note: Values are mean ± SD (n=3)

Table No. 6: Stability study of Fe_2O_3-NPs gel

Parameter	Fe_2O_3-NPs gel (40 ℃ ± 2 ℃/ 75% ± 5 RH)		
	30 Days	60 Days	90 Days
Color	light brown	light brown	light brown
Odor	No	No	No
pH	5.6 ± 0.16	5.5 ± 0.32	5.39 ± 0.24

Note: Values are mean ± SD (n=3)

CONCLUSION

The current work, which aimed to produce honey-based gels containing ZnO-NPs and Fe_2O_3-NPs for wound healing applications, was effectively completed. Comprehensively, the results show that the precipitation method was effective in the production of ZnO-NPs and Fe_2O_3-NPs. UV-vis, FTIR, SEM and zeta potential analysis confirmed the size of the NPs was at the nanoscale, their shape was excellent and they were stable. The reason behind using honey as a natural gel foundation is its ability to serve as an antibacterial, antioxidant, and wound-healing ingredient when used with NPs. The gels met the ICH requirements of pH, viscosity, spreadability, and stability and were suitable for topical application. The *in vivo* wound healing studies on Wistar rats demonstrated that the ZnO-NPs and Fe_2O_3-NPs gels had dramatic wound contraction, collagen deposition, and re-epithelialization improvements in comparison with the control and plain gels. These findings were supported by histopathological tests, which revealed that there was less inflammation, increased fibroblast proliferation, and better tissue organization in the treated groups. The results reveal that honey gels containing NPs significantly enhanced wound healing and antibacterial properties as compared to the control and plain gels. These findings suggest that honey-based gels relying on ZnO-NPs and Fe_2O_3-NPs could be considered as a potential solution when handling effective topical wound care. ZnO-NPs gel demonstrated improvement in terms of healing activity and wound healing faster by the 21st day and a reduction in inflammation. Honey gels containing NPs are a safe, effective, and prospective method of advanced wound care. ZnO-NPs gel is the best formulation.

ABBREVIATIONS

ZnO-NPs: Zinc Oxide Nanoparticles; Fe_2O_3-NPs: Iron Oxide Nanoparticles; NPs: Nanoparticles; UV-Vis: Ultraviolet-Visible Spectroscopy; FTIR: Fourier Transform Infrared Spectroscopy; SEM: Scanning Electron Microscopy; TEM: Transmission Electron Microscopy; DLS: Dynamic Light Scattering; MIC: Minimum Inhibitory Concentration; SPR: Surface Plasmon Resonance; ROS: Reactive Oxygen Species; ICH: International Council for Harmonisation; TEA: Triethanolamine; NaOH: Sodium Hydroxide; DMSO: Dimethyl Sulphoxide; rpm: Revolutions Per Minute; nm: Nanometer; µg/mL: Microgram per Milliliter; mM: Millimolar; ℃: Degree Celsius; RH: Relative Humidity; SD: Standard Deviation; w/w: Weight by Weight; ELISA: Enzyme-Linked Immunosorbent Assay

ACKNOWLEDGEMENT

The authors are grateful to the Principal of Maratha Mandal's College of Pharmacy, Belagavi, and the Management of MM Group of Institutions for the provision of research facilities and support. We also thank King Faisal University and Dar Al Uloom

University for their institutional support throughout this study.

FUNDING

Funding: This work was supported by the Deanship of Scientific Research, Vice Presidency for Graduate Studies and Scientific Research, King Faisal University, Saudi Arabia [Grant No. KFU261186]

CONFLICT OF INTEREST

The authors declare no conflict of interest.

REFERENCES

1. Sabale P, Bhimani B, Prajapati C, Sabalea V. An overview of medicinal plants as wound healers. Journal of Applied Pharmaceutical Science. 2012 Nov 30;2(11):143-50.
2. Pourmadadi M, Rahmani E, Shamsabadipour A, Mahtabian S, Ahmadi M, Rahdar A, Díez-Pascual AM. Role of iron oxide (Fe2O3) nanocomposites in advanced biomedical applications: a state-of-the-art review. Nanomaterials. 2022 Nov 2;12(21):3873.
3. Lin PH, Sermersheim M, Li H, Lee PH, Steinberg SM, Ma J. Zinc in wound healing modulation. Nutrients. 2017 Dec 24;10(1):16.
4. Wang Z, Cui X, Hao G, He J. Aberrant expression of PI3K/AKT signaling is involved in apoptosis resistance of hepatocellular carcinoma. Open life sciences. 2021 Sep 27;16(1):1037-44.
5. Rodrigues M, Gurtner GC. Black, white, and gray: macrophages in skin repair and disease. Current pathobiology reports. 2017 Dec;5(4):333-42.
6. Wynn M. The impact of infection on the four stages of acute wound healing: an overview. Wounds UK. 2021 Jun 1;17(2).
7. Noronha A, Modamio J, Jarosz Y, Guerard E, Sompairac N, Preciat G, Daníelsdóttir AD, Krecke M, Merten D, Haraldsdóttir HS, Heinken A. The Virtual Metabolic Human database: integrating human and gut microbiome metabolism with nutrition and disease. Nucleic acids research. 2019 Jan 8;47(D1): D614-24.
8. Tottoli EM, Dorati R, Genta I, Chiesa E, Pisani S, Conti B. Skin wound healing process and new emerging technologies for skin wound care and regeneration. Pharmaceutics. 2020 Aug 5;12(8):735.
9. Bianchera A, Catanzano O, Boateng J, Elviri L. The place of biomaterials in wound healing. Therapeutic dressings and wound healing applications. 2020 Mar 2:337-66.
10. Boateng J, Catanzano O. Advanced therapeutic dressings for effective wound healing—a review. Journal of pharmaceutical sciences. 2015 Nov 1;104(11):3653-80.
11. Mandal MD, Mandal S. Honey: its medicinal property and antibacterial activity. Asian Pacific journal of tropical biomedicine. 2011 Apr 1;1(2):154-60.
12. Dhivya S, Padma VV, Santhini E. Wound dressings–a review. BioMedicine. 2015 Nov 28;5(4):22.
13. Lansdown AB, Mirastschijski U, Stubbs N, Scanlon E, Ågren MS. Zinc in wound healing: theoretical, experimental, and clinical aspects. Wound repair and regeneration. 2007 Jan;15(1):2-16.
14. Zhou Q, Fu L, Zhu J. Electrochemical sensors go nano: Carbon nanomaterials for ultrasensitive heavy metal analysis. Current Nanoscience. 2025 Jul;21(4):596-612.
15. Shi Z, Yao C, Shui Y, Li S, Yan H. Research progress on the mechanism of angiogenesis in wound repair and regeneration. Frontiers in physiology. 2023 Nov 27;14: 1284981.
16. Chen M, Liu T, Wang X, Gao L, Cheng Y, Jiang J, Zhang J. Comprehensive wound healing using ETN@ Fe7S8 complex by positively regulating multiple programmed phases. Journal of Nanobiotechnology. 2025 May 13;23(1):342.
17. Gushiken LF, Beserra FP, Bastos JK, Jackson CJ, Pellizzon CH. Cutaneous wound healing: An update from physiopathology to current therapies. Life. 2021 Jul 7;11(7):665.
18. Wang H, Xu Z, Li Q, Wu J. Application of metal-based biomaterials in wound repair. Engineered regeneration. 2021 Jan 1; 2:137-53.
19. Pourmadadi M, Rahmani E, Shamsabadipour A, Mahtabian S, Ahmadi M, Rahdar A, Díez-Pascual AM. Role of iron oxide (Fe2O3) nanocomposites in advanced biomedical applications: a state-of-the-art review. Nanomaterials. 2022 Nov 2;12(21):3873.
20. Giusto G, Vercelli C, Comino F, Caramello V, Tursi M, Gandini M. A new, easy-to-make pectin-honey hydrogel enhances wound healing in rats. BMC complementary and alternative medicine. 2017 May 16;17(1):266.
21. Zainuddin AN, Mustakim NN, Rosemanzailani FA, Fadilah NI, Maarof M, Fauzi MB. A comprehensive review of honey-containing hydrogel for wound healing applications. Gels. 2025 Mar 12;11(3):194.

22. WAYAL V, NV T. Assessment of wound healing activity of potent herbal extracts gel in albino Wistar rat. ASSESSMENT. 2022;15(8).
23. El-Kased RF, Amer RI, Attia D, Elmazar MM. Honey-based hydrogel: In vitro and comparative In vivo evaluation for burn wound healing. Scientific reports. 2017 Aug 29;7(1):9692.
24. Manuja A, Kumar B, Chhabra D, Brar B, Thachamvally R, Pal Y, Prasad M. Synergistic effect of zinc-chitosan nanoparticles and hydroxychloroquine to inhibit buffalo coronavirus. Polymers. 2023 Jul 5;15(13):2949.
25. Kumar SS, Venkateswarlu P, Rao VR, Rao GN. Synthesis, characterization and optical properties of zinc oxide nanoparticles. International Nano Letters. 2013 Dec;3(1):30.
26. Mohammed KM. Al khazraji, HA Synthesis and characterization of α-Fe2O3 nanoparticles using the precipitation and eco-friendly methods. J. Pharm. Negative Results. 2022; 13:782-9.
27. Cabrera MP, Assis CR, Neri DF, Pereira CF, Soria F, Carvalho Jr LB. High sucrolytic activity by invertase immobilized onto magnetic diatomaceous earth nanoparticles. Biotechnology reports. 2017 Mar 1; 14:38-46.
28. Bakil SN, Kamal H, Abdullah HZ, Idris MI. Sodium alginate-zinc oxide nanocomposite film for antibacterial wound healing applications. Biointerface Res. Appl. Chem. 2020;10(2):6245-52.
29. Yun TJ, Oh WB, Lee BR, Liang ZL, Park MH, Kim IS. A numerical study on particle behaviors of fluid flow in pulverizer. Materials Today: Proceedings. 2020 Jan 1; 22:1939-48.
30. Chikezie IO. Determination of minimum inhibitory concentration (MIC) and minimum bactericidal concentration (MBC) using a novel dilution tube method. African journal of microbiology research. 2017 Jun 21;11(23):977-80.
31. Meena A, Ramana PV. High-rise structural stalling and drift effect owe to lateral loading. Materials Today: Proceedings. 2022 Jan 1; 52:1472-8.
32. Khan AW, Kotta S, Ansari SH, Sharma RK, Kumar A, Ali J. Formulation development, optimization and evaluation of aloe vera gel for wound healing. Pharmacognosy magazine. 2013 Oct;9(Suppl 1): S6.
33. Noman MA, Alburyhi MM, Saif AA, Yahya TA. Formulation and Evaluation of Polyherbal Extract for Skin Hyperpigmentation as Gel Advanced Delivery Systems. World Journal of Pharmaceutical Research. 2024 Oct 4;13(22):1260-80.
34. Roy K, Chakraborty M, Theengh A. Evaluation of wound healing activity of hydroalcoholic extract of Ficus glomerata on Wistar albino rats. *Int J Pharm Sci Res*. 2021;12(1):554–558. doi:10.13040/IJPSR.0975-8232.12(1).554-558.
35. Murthy S, Gautam MK, Goel S, Purohit V, Sharma H, Goel RK. Evaluation of in vivo wound healing activity of Bacopa monniera on different wound model in rats. BioMed research international. 2013;2013(1):972028.
36. Kantipudi S, Sunkara JR, Rallabhandi M, Thonangi CV, Cholla RD, Kollu P, Parvathaneni MK, Pammi SV. Enhanced wound healing activity of Ag–ZnO composite NPs in Wistar Albino rats. IET nanobiotechnology. 2018 Jun;12(4):473-8.
37. Nagar HK, Srivastava AK, Srivastava R, Kurmi ML, Chandel HS, Ranawat MS. Pharmacological investigation of the wound healing activity of Cestrum nocturnum (L.) ointment in Wistar albino rats. Journal of pharmaceutics. 2016;2016(1):9249040.
38. Mahlangu ZP, Botha FS, Madoroba E, Chokoe K, Elgorashi EE. Antimicrobial activity of Albizia gummifera (JF Gmel.) CA Sm leaf extracts against four Salmonella serovars. South African Journal of Botany. 2017 Jan 1; 108:132-6. Dantas MG, Reis SA, Damasceno CM, Rolim LA, Rolim-Neto PJ, Carvalho FO, et al. Stability evaluation of borneol gel. *Sci World J*. 2016; 2016:7394685. doi:10.1155/2016/7394685.
39. Babu PJ, Doble M, Raichur AM. Silver oxide nanoparticles embedded silk fibroin spuns: Microwave mediated preparation, characterization and their synergistic wound healing and anti-bacterial activity. Journal of colloid and interface science. 2018 Mar 1; 513:62-71.
40. Ghorpade DD. Formulation and evaluation of microsponge-loaded topical gel. *Drug Dev Res*. 2023;84(5):1–10. doi:10.1002/ddr.22351.
41. Raghupathi KR, Koodali RT, Manna AC. Size-dependent bacterial growth inhibition and mechanism of antibacterial activity of zinc oxide nanoparticles. Langmuir. 2011 Apr 5;27(7):4020-8..
42. Mahanty A, Mishra S, Bosu R, Maurya UK, Netam SP, Sarkar B. Phytoextract-synthesized iron oxide nanoparticles inhibit bacterial growth and biofilm formation. J Nanomater. 2019; 2019:1–10. doi:10.1155/2019/5985029.